Journal of Systems Engineering and Electronics
Vol. 31, No. 6, December 2020, pp.1193 – 1205

Observability and estimability of passive radar with unknown illuminator states using different observations

JING Tong, TIAN Wei*, HUANG Gaoming, and PENG Huafu

College of Electronic Engineering, Naval University of Engineering, Wuhan 430033, China

Abstract: Most existing studies about passive radar systems are based on the already known illuminator of opportunity (IO) states. However, in practice, the receiver generally has little knowledge about the IO states. Little research has studied this problem. This paper analyzes the observability and estimability for passive radar systems with unknown IO states under three typical scenarios. Besides, the directions of high and low estimability with respect to various states are given. Moreover, two types of observations are taken into account. The effects of different observations on both observability and estimability are well analyzed. For the observability test, linear and nonlinear methods are considered, which proves that both tests are applicable to the system. Numerical simulations confirm the correctness of the theoretical analysis.

Keywords: passive radar, passive coherent location (PCL), observability, estimability, unknown illuminator states.

DOI: 10.23919/JSEE.2020.000092

1. Introduction

Passive radar works with the help of non-cooperative illuminators of opportunity (IOs), which is also called passive coherent location (PCL) system [1−6]. Compared with the conventional active counterparts that use their own dedicated transmitters, passive radar has a number of advantages, such as easy construction, spectrum saving, and significant performance improvement with multi-static configuration. However, since the receiver generically has no prior knowledge of the IO waveform, one may have difficulty gaining the aforementioned superiorities. Hence, intensive attention has been paid to the research filed on passive radar systems.

Target localization and tracking are hot research topics in passive radar. In [7] and [8], two joint delay-Doppler estimators were proposed, where the direct-path interference (DPI) to the surveillance channel was taken into account. The direct-path delay was compensated based on the assumption that the IO location has been obtained for simplifying the problem model. Abdullah et al. [9] proved that the passive radar utilizing the stationary long-term evolution (LTE) communication station as IO could offer a satisfying performance on moving vehicle tracking. To the best of our knowledge, almost all existing studies assume that the IO location is fixed and exactly known. However, such an assumption deviates from the real situation. For instance, the passive radar may be required to promptly deploy in some unfamiliar areas. Therefore, little knowledge about the IO states, such as the IO location, could be provided to the receiver in advance. Hence, the system has to simultaneously estimate the states of both the IO and targets for its radar function. Herein, the problem is regarded as the simultaneous localization and mapping (SLAM) or opportunistic navigation (OpNav) problem [10]. In contrast to these two problems, the environment in the passive radar is more complex since the IO states are dynamic. Therefore, studying the target localization and tracking problems without the knowledge of the IO states is extremely necessary. First of all, we should find out whether such problems have solvability. This paper aims to make a detailed analysis of the observability in passive radar systems with unknown IO states. Simultaneously, the degree of observability, i.e., estimability, is considered.

Observability is an important concept. When the system is observable, a unique solution about the system states can be obtained [11]. In general, a passive radar system is nonlinear. Several major methods for nonlinear observability analysis are concluded as follows. First, the geometric approach extracts the information associated with the parameters of target motion. Rao [12] adopted an elementary geometry method to analyze the observability of an observer with a multi-leg trajectory in a bearings-only system. Based on the similar analysis, a method to

Manuscript received September 23, 2019.
*Corresponding author.
This work was supported by the National Natural Science Foundation of China (61803379) and the China Postdoctoral Science Foundation (2017M613370; 2018T111129).

calculate the target range using bearings-only measurement was given in [13]. Second, the linear observability test that converts the nonlinear system model into its pseudo-linear form may be exploited to nonlinear observability analysis. Jauffret et al. [14] proved that the necessary and sufficient condition for the system to be observable over a given finite time period is the so-called Gram matrix reversible. Since the Gram matrix is computationally intractable, Becker [15] gave an equivalent but more simple criterion. Song [16] extended such analysis to a broader target motion model. Finally, the nonlinear observability test is the most common analysis tool for nonlinear systems, in which two methods are typically used. One is the extension of the linear Gram matrix criterion, where relative Jacobian matrices are utilized to take the place of the state transition and observation matrices [17]. The other is based on examining the Fisher information matrix (FIM) [18−21]. Besides, some research studied the observability by constructing the piece-wise constant system (PWCS) model [22−27].

In this work, the observability and estimability for passive radar systems are studied. The contributions of this paper are given as follows. First, different from most existing research with already known IO states, the observability with unknown and dynamic IO states in three typical scenarios is analyzed, which demonstrates whether the system in each scenario is observable. Second, associated estimability is also studied by decomposing the error covariance matrix of the extended Kalman filter (EKF). Third, we consider the effect of two different types of observations on both observability and estimability. Fourth, two observability analysis methods, linear and nonlinear observability tests, are applied. Theoretical analysis proves that both tests are applicable to the system. Finally, experimental results validate the correctness of the theoretical analysis and illustrate that the IO and target states can be simultaneously estimated. It is worth pointing out that Guo et al. [28] studied a similar problem about the observability without experimental validation, where the necessary and sufficient conditions for local observability are derived based on FIM. This paper extends the work of [28] in four different ways. First, the observability under more configurations is considered. Second, starting from the rigorous local properties of observability, both linear and nonlinear observability tests are used, which may have less computation than the method in [28]. Importantly, simulation experiments are given to confirm the correctness of our analysis. Third, we additionally analyze the corresponding estimability. Finally, the effect of different observations on the system is also studied.

The rest of the paper is organized as follows. In Section 2, the problem model is given. In Section 3, the linear and nonlinear observability test tools are studied. Besides, the observability analysis with unknown IO states using different observations is deduced. Section 4 introduces a method to analyze system estimability. Simulation results are illustrated in Section 5.

2. Problem formulation

We consider three typical cases in passive radar systems: (i) single receiver with single target and single IO (SRSTSIO), (ii) single receiver with multiple targets and single IO (SRMTSIO), and (iii) single receiver with single target and multiple IOs (SRSTMIOs). Both target and IO states are dynamic and unknown to the receiver. Herein, only one receiver with the state $\boldsymbol{X}_r = [\boldsymbol{p}_r^{\mathrm{T}}, \dot{\boldsymbol{p}}_r^{\mathrm{T}}]^{\mathrm{T}}$ is considered, where $\boldsymbol{p}_r = [x_r, y_r]^{\mathrm{T}}$ and $\dot{\boldsymbol{p}}_r = [\dot{x}_r, \dot{y}_r]^{\mathrm{T}}$ are associated location and velocity states, respectively. We assume that the receiver states are exactly known. Moreover, the system will not lose the measurements of the targets and IOs during the receiver observation period.

2.1 State model

Suppose that M IOs and N targets are in the surveillance area. They all maneuver with the nearly constant velocity (NCV) model. Let $\boldsymbol{X}_{t,i} = [\boldsymbol{p}_{t,i}^{\mathrm{T}}, \dot{\boldsymbol{p}}_{t,i}^{\mathrm{T}}]^{\mathrm{T}}$ with $\boldsymbol{p}_{t,i} = [x_{t,i}, y_{t,i}]^{\mathrm{T}}$ be the state of the ith IO. $\boldsymbol{X}_{g,j} = [\boldsymbol{p}_{g,j}^{\mathrm{T}}, \dot{\boldsymbol{p}}_{g,j}^{\mathrm{T}}]^{\mathrm{T}}$ with $\boldsymbol{p}_{g,j} = [x_{g,j}, y_{g,j}]^{\mathrm{T}}$ is designated as the state of the jth target. Hence, the discrete-time (DT) IO state model with the sampling interval T_s is

$$\boldsymbol{X}_t(k+1) = \boldsymbol{F}_t \boldsymbol{X}_t(k) + \boldsymbol{w}_t(k) \tag{1}$$

where $\boldsymbol{w}_t$ is the IO process noise vector, which is assumed to be a zero-mean unrelated Gaussian white noise sequence with the covariance $\boldsymbol{Q}_t$. $\boldsymbol{F}_t$ is the state transition matrix, which is denoted as

$$\boldsymbol{F}_t = \begin{bmatrix} 1 & 0 & T_s & 0 \\ 0 & 1 & 0 & T_s \\ 0 & 0 & 1 & 0 \\ 0 & 0 & 0 & 1 \end{bmatrix}.$$

It should be noted that when a single IO exists, $\boldsymbol{X}_t$ is equal to $\boldsymbol{X}_{t,1}$. While considering multiple IOs, $\boldsymbol{X}_t$ will be augmented to $\boldsymbol{X}_t = [\boldsymbol{X}_{t,1}^{\mathrm{T}}, \boldsymbol{X}_{t,2}^{\mathrm{T}}, \cdots, \boldsymbol{X}_{t,M}^{\mathrm{T}}]^{\mathrm{T}}$. Then the associated state transition matrix $\boldsymbol{F}_t'$ and the process noise covariance $\boldsymbol{Q}_t'$ are augmented to diagonal matrices with diagonal elements composed of $\boldsymbol{F}_t$ and $\boldsymbol{Q}_t$, respectively, i.e.,

$$\boldsymbol{F}_t' = \begin{bmatrix} \boldsymbol{F}_{t,1} & & & \\ & \boldsymbol{F}_{t,2} & & \\ & & \ddots & \\ & & & \boldsymbol{F}_{t,M} \end{bmatrix}$$

and

$$\boldsymbol{Q}_t' = \begin{bmatrix} \boldsymbol{Q}_{t,1} & & & \\ & \boldsymbol{Q}_{t,2} & & \\ & & \ddots & \\ & & & \boldsymbol{Q}_{t,M} \end{bmatrix}.$$

Similarly, the DT target state model is defined as

$$\boldsymbol{X}_g(k+1) = \boldsymbol{F}_g \boldsymbol{X}_g(k) + \boldsymbol{w}_g(k) \tag{2}$$

where $\boldsymbol{F}_g = \boldsymbol{F}_t$ is the state transition matrix of the target, $\boldsymbol{w}_g$ is a zero-mean unrelated Gaussian white noise sequence with the covariance $\boldsymbol{Q}_g$. While multiple targets are taken into account, variables in the target state model are similarly augmented as the case with multiple IOs.

For the observability analysis, the system state is designated as $\boldsymbol{X} = [\boldsymbol{X}_t^{\mathrm{T}}, \boldsymbol{X}_g^{\mathrm{T}}]^{\mathrm{T}}$. Hence, the system state model is

$$\boldsymbol{X}(k+1) = \boldsymbol{F}\boldsymbol{X}(k) + \boldsymbol{w}(k) \tag{3}$$

where $\boldsymbol{F} = \mathrm{diag}[\boldsymbol{F}_t, \boldsymbol{F}_g]$; $\boldsymbol{w} = [\boldsymbol{w}_t^{\mathrm{T}}, \boldsymbol{w}_g^{\mathrm{T}}]^{\mathrm{T}}$ is a zero-mean unrelated Gaussian white noise sequence with the covariance $\boldsymbol{Q} = \mathrm{diag}[\boldsymbol{Q}_t, \boldsymbol{Q}_g]$.

2.2 Observation model

In this problem, all the observations from the target and the IO should be centrally processed at the receiver with an appropriate filter. Herein, for clarity, we define the observation only produced by the IO as the IO observation (IOO) and the observation related to the target as the target observation (TO), respectively. Hence, the whole system observations are composed of IOOs and TOs. Assume that the IOO is only the angle of arrival (AOA). Let α_i be the AOA observation generated by the ith IO, where $i = 1, 2, \cdots, M$. Whereby,

$$\alpha_i = \arctan \frac{y_{t,i} - y_r}{x_{t,i} - x_r}. \tag{4}$$

Two types of TOs are considered in this paper. One is based on single observation from the target (SOT). The other utilizes joint observation from the target (JOT). In the conventional passive location that only collects signals emitted by the target, single observation with Doppler difference can determine both the target's range and velocity. Compared with other observations, such as AOA that can only give the direction of the target motion, Doppler difference is more attractive in practice. Hence, for the SOT case, the TO only contains the Doppler difference information. Therefore, let $f_{d,ij}$ be the Doppler difference in terms of the jth target associated with the ith IO [29], where $i = 1, 2, \cdots, M$, $j = 1, 2, \cdots, N$. Then

$$f_{d,ij} = -\frac{f_{c,i}}{\mathrm{c}} \left[\frac{(\boldsymbol{p}_r - \boldsymbol{p}_{g,j})^{\mathrm{T}} (\dot{\boldsymbol{p}}_r - \dot{\boldsymbol{p}}_{g,j})}{\|\boldsymbol{p}_r - \boldsymbol{p}_{g,j}\|_2} + \frac{(\boldsymbol{p}_{g,j} - \boldsymbol{p}_{t,i})^{\mathrm{T}} (\dot{\boldsymbol{p}}_{g,j} - \dot{\boldsymbol{p}}_{t,i})}{\|\boldsymbol{p}_{g,j} - \boldsymbol{p}_{t,i}\|_2} - \frac{(\boldsymbol{p}_{t,j} - \boldsymbol{p}_r)^{\mathrm{T}} (\dot{\boldsymbol{p}}_{t,j} - \dot{\boldsymbol{p}}_r)}{\|\boldsymbol{p}_{t,j} - \boldsymbol{p}_r\|_2} \right] \tag{5}$$

where $f_{c,i}$ is the carrier frequency of the ith IO, c is the speed of light, $\|\cdot\|_2$ represents the 2-norm operator. For the JOT case, the AOA from the target and time of arrival (TOA) [30] are considered, the reasons of which are given as follows. First, computing the observability matrix will be more intractable if the observation vector is augmented based on the Doppler difference. Second, the calculation of the Jacobian matrix of the AOA is relatively simple. However, the expression of the target AOA has no relationship with the IO. Hence, only using target AOA observation will make the problem identical to target tracking with bearing-only measurements. Finally, the TOA observation is absorbed in order to simplify the computation and make the observation related to the IO states, which can also improve the tracking performance in practical applications when the carrier frequency of the IO is low [30,31]. Let β_j be the AOA from the jth target, and ρ_{ij} be the TOA from the ijth IO-target pair, where $i = 1, 2, \cdots, M$, $j = 1, 2, \cdots, N$. Hence,

$$\beta_j = \arctan \frac{y_{g,j} - y_r}{x_{g,j} - x_r}, \tag{6}$$

$$\rho_{ij} = \|\boldsymbol{p}_r - \boldsymbol{p}_{g,j}\|_2 + \|\boldsymbol{p}_{g,j} - \boldsymbol{p}_{t,i}\|_2. \tag{7}$$

Therefore, two types of the system observation model are

$$\boldsymbol{Z}_s(k+1) = \boldsymbol{h}_s[\boldsymbol{X}(k+1)] + \boldsymbol{v}_s(k+1), \tag{8}$$

$$\boldsymbol{Z}_o(k+1) = \boldsymbol{h}_o[\boldsymbol{X}(k+1)] + \boldsymbol{v}_o(k+1), \tag{9}$$

where $\boldsymbol{Z}_s = [\boldsymbol{\alpha}^{\mathrm{T}}, \boldsymbol{f}_d^{\mathrm{T}}]^{\mathrm{T}}$ is the observation vector in terms of the SOT case with $\boldsymbol{\alpha} = [\alpha_1, \cdots, \alpha_M]^{\mathrm{T}}$ and $\boldsymbol{f}_d = [f_{d,11}, \cdots, f_{d,MN}]^{\mathrm{T}}$; $\boldsymbol{v}_s$ is the observation noise, which is assumed to be a zero-mean unrelated white Gaussian noise sequence with the covariance $\boldsymbol{R}_s = \mathrm{diag}[\sigma_{\alpha_1}^2, \cdots, \sigma_{\alpha_M}^2, \sigma_{f_{d,11}}^2, \cdots, \sigma_{f_{d,MN}}^2]$; $\boldsymbol{Z}_o = [\boldsymbol{\alpha}^{\mathrm{T}}, \boldsymbol{\rho}^{\mathrm{T}}, \boldsymbol{\beta}^{\mathrm{T}}]^{\mathrm{T}}$ is the observation vector in terms of the JOT case with $\boldsymbol{\rho} = [\rho_{11}, \cdots, \rho_{MN}]^{\mathrm{T}}$ and $\boldsymbol{\beta} = [\beta_1, \cdots, \beta_N]^{\mathrm{T}}$; $\boldsymbol{v}_o$ is assumed to be a zero-mean unrelated white Gaussian noise sequence with the covariance $\boldsymbol{R}_o = \mathrm{diag}[\sigma_{\alpha_1}^2, \cdots, \sigma_{\alpha_M}^2, \sigma_{\rho_{11}}^2, \cdots, \sigma_{\rho_{MN}}^2, \sigma_{\beta_1}^2, \cdots, \sigma_{\beta_N}^2]$, where σ is the corresponding observation noise.

3. Observability test and analysis

If the initial state of a system can be uniquely determined by the system output with a given input function, such a system will be treated as observable [32]. In this paper, linear and nonlinear observability tests [33] are applied to determining whether the system in each scenario with dif-

ferent observations is observable.

3.1 Observability test

3.1.1 Nonlinear observability test

For a nonlinear system, the global observability is difficult to establish since the system may distinguish between initial conditions over a long period of time. Hence, local properties are more applicable [33,34]. Particularly, a system is supposed to be instantaneously observable in a certain neighborhood of the state trajectories [35]. Besides, it is suitable to utilize the nonlinear observability test to analyze nonlinear systems, which may better reflect the characteristics of the systems. Therefore, an observability algebraic test based on establishing local weak observability of the nonlinear system with its control affine form is applied [36]. The control affine form of a continuous-time (CT) nonlinear system can be written as

$$\sum_{NL}:\begin{cases}\dot{\boldsymbol{X}}(t)=\boldsymbol{f}_0[\dot{\boldsymbol{X}}(t)]+\sum_{i=1}^{r}\boldsymbol{f}_i[\dot{\boldsymbol{X}}(t)]u_i\\ \boldsymbol{Z}(t)=\boldsymbol{h}[\boldsymbol{X}(t)]\end{cases}\tag{10}$$

where $\boldsymbol{X}$ is the state vector, $\boldsymbol{Z}$ is the observation vector, $\boldsymbol{f}$ is the state function, $\boldsymbol{h}$ is the observation function, and $\boldsymbol{u}$ is the control input vector. The algebraic test establishes the local weak observability by constructing a nonlinear observability matrix with the Lie derivative. Such a nonlinear observability matrix is calculated as

$$\boldsymbol{\Gamma}_{NL}=\nabla_X[L_f^0\boldsymbol{h}(\boldsymbol{X}),L_f^1\boldsymbol{h}(\boldsymbol{X}),\cdots,L_f^{n-1}\boldsymbol{h}(\boldsymbol{X})]^{\mathrm{T}}\tag{11}$$

where ∇_X represents the gradient according to the system state $\boldsymbol{X}$, n is the dimension of $\boldsymbol{X}$, $\boldsymbol{f}=[\boldsymbol{f}_1,\boldsymbol{f}_2,\cdots,\boldsymbol{f}_n]^{\mathrm{T}}$ is the vector of state function, $\boldsymbol{h}=[\boldsymbol{h}_1,\boldsymbol{h}_2,\cdots,\boldsymbol{h}_m]^{\mathrm{T}}$ is the vector of observation function, and m is the dimension of $\boldsymbol{Z}$. The calculation rules of Lie derivative is defined as

$$L_f^0\boldsymbol{h}(X)=\boldsymbol{h}(X),\tag{12}$$

$$L_f^1\boldsymbol{h}(X)=\langle\nabla_X\boldsymbol{h}(\boldsymbol{X}),\boldsymbol{f}(\boldsymbol{X})\rangle,\tag{13}$$

$$L_f^2\boldsymbol{h}(X)=\langle[\nabla_X L_f^1\boldsymbol{h}(\boldsymbol{X})],\boldsymbol{f}(\boldsymbol{X})\rangle,\tag{14}$$

where $\langle\cdot\rangle$ is the inner product operator.

It is worth noting that a system $\sum_{NL}$ is locally weakly observable at $\boldsymbol{X}=\boldsymbol{X}_0$ if the nonlinear observability matrix $\boldsymbol{\Gamma}_{NL}$ is full rank [10,37].

3.1.2 Linear observability test

Consider a DT linear time-varying (LTV) system denoted as

$$\sum_{L}:\begin{cases}\boldsymbol{X}(k+1)=\boldsymbol{F}(k)\boldsymbol{X}(k)+\boldsymbol{G}(k)\boldsymbol{u}(k)\\ \boldsymbol{Z}(k)=\boldsymbol{H}(k)\boldsymbol{X}(k)\end{cases}\tag{15}$$

where $\boldsymbol{X}(k)$ is the n-dimensional state vector, $\boldsymbol{Z}(k)$ is the m-dimensional observation vector, and $\boldsymbol{u}(k)$ is the r-dimensional control vector. $\boldsymbol{F}(k)$, $\boldsymbol{H}(k)$ and $\boldsymbol{G}(k)$ are matrices with $n\times n$, $m\times n$, and $n\times r$ dimensions, respectively.

A linear system $\sum_{L}$ is said to be completely observable if the linear observability matrix, denoted by $\boldsymbol{\Gamma}_L$, is full-rank for all values of k [38], where $\boldsymbol{\Gamma}_L$ is calculated as

$$\boldsymbol{\Gamma}_L=\begin{bmatrix}\boldsymbol{H}(k)\\ \boldsymbol{H}(k+1)\boldsymbol{F}(k)\\ \boldsymbol{H}(k+2)\boldsymbol{F}(k+1)\boldsymbol{F}(k)\\ \vdots\\ \boldsymbol{H}(k+n-1)\boldsymbol{F}(k+n-2)\cdots\boldsymbol{F}(k)\end{bmatrix}.\tag{16}$$

However, we focus on the local observability rather than global observability. Here, we utilize the l-step observability matrix to furnish the local observability of $\sum_{L}$ [27,39]. The matrix defined in (16) is rewritten as

$$\boldsymbol{\Gamma}_L(k,k+l)=\begin{bmatrix}\boldsymbol{H}(k)\\ \boldsymbol{H}(k+1)\boldsymbol{F}(k)\\ \boldsymbol{H}(k+2)\boldsymbol{F}(k+1)\boldsymbol{F}(k)\\ \vdots\\ \boldsymbol{H}(k+l-1)\boldsymbol{F}(k+l-2)\cdots\boldsymbol{F}(k)\end{bmatrix}.\tag{17}$$

The system $\sum_{L}$ is locally l-step observable over the time period from k to $k+l-1$ if and only if the matrix $\boldsymbol{\Gamma}_L(k,k+l)$ is full rank.

Note that the nonlinear system defined in Section 2 should be changed to its linearized error form for applying this linear test [27].

3.2 Observability analysis with unknown IO states

The observability of passive radar systems with unknown IO states using different observations under three typical cases is analyzed in this subsection. Based on the two observability tests, we will prove whether the system in each scenario is observable.

3.2.1 Geometry singularity

We assume that the receiver, target, and IO are not collinear in the forthcoming analysis since the observability matrix will lose rank. A simple example will be given to prove this point.

Consider a non-collinear SRSTSIO case, where the system has prior knowledge of the IO initial states.

Hence, the system state is defined as $\boldsymbol{X}=[\boldsymbol{X}_t^{\mathrm{T}},\boldsymbol{X}_g^{\mathrm{T}}]^{\mathrm{T}}=[x_t,y_t,\dot{x}_t,\dot{y}_t,x_g,y_g,\dot{x}_g,\dot{y}_g]^{\mathrm{T}}$, the dimension of which is eight. The observation vector is $\boldsymbol{Z}_s=[\boldsymbol{X}_t,\alpha,f_d]^{\mathrm{T}}$ for SOT and $\boldsymbol{Z}_o=[\boldsymbol{X}_t,\alpha,\rho,\beta]^{\mathrm{T}}$ for JOT, respectively [10].

(i) Analysis with SOT. For the nonlinear observability test, the only linearly independent rows are $\left\{\nabla_{\boldsymbol{X}}^{\mathrm{T}}[L_{f_0}^0\boldsymbol{h}_q(\boldsymbol{X})],\ q=1,2,3,4;\ \nabla_{\boldsymbol{X}}^{\mathrm{T}}[L_{f_0}^p\boldsymbol{h}_6(\boldsymbol{X})],p=0,1,2,3\right\}$ in terms of the matrix $\boldsymbol{\Gamma}_{NL}$. Hence, $\mathrm{rank}(\boldsymbol{\Gamma}_{NL})=8$, which means the system has the local weak observability.

For the linear observability test, the observation vector $\boldsymbol{Z}_s$ leads to the Jacobian matrix denoted as

$$\boldsymbol{H}(k)=\begin{bmatrix}\boldsymbol{I}_{4\times4} & \boldsymbol{0}\\ \boldsymbol{\zeta}_{r,t}(k) & \boldsymbol{0}\\ \boldsymbol{U}_{r,t,g}(k) & \boldsymbol{O}_{r,t,g}(k)\end{bmatrix} \tag{18}$$

where $\boldsymbol{I}_{4\times4}$ is the unit matrix, $\boldsymbol{\zeta}_{r,t}(k)=[-B_{t,r}(k),A_{t,r}(k),0,0]$ is the derivative of the IO AOA observation α to the IO states, $\boldsymbol{U}_{r,t,g}(k)=[^{p_t}U_{r,t,g}(k),^{\dot{p}_t}U_{r,t,g}(k)]$ is the derivative of the Doppler difference f_d to the IO states, $\boldsymbol{O}_{r,t,g}(k)=[^{p_g}O_{r,t,g}(k),^{\dot{p}_g}O_{r,t,g}(k)]$ is the derivative of f_d to the target states, where

$$^{p_t}U_{r,t,g}(k)=-\frac{f_c}{\mathrm{c}}\left[\left(\frac{^{x}\Omega_{t,g}(k)-\delta_{g,t}^{A}(k)}{\|\boldsymbol{p}_g(k)-\boldsymbol{p}_t(k)\|_2^2}-\frac{^{x}\Omega_{t,r}(k)-\delta_{t,r}^{A}(k)}{\|\boldsymbol{p}_t(k)-\boldsymbol{p}_r(k)\|_2^2}\right)\cdot\left(\frac{^{y}\Omega_{t,y}(k)-\delta_{g,t}^{B}(k)}{\|\boldsymbol{p}_g(k)-\boldsymbol{p}_t(k)\|_2^2}-\frac{^{y}\Omega_{t,r}(k)-\delta_{t,r}^{B}(k)}{\|\boldsymbol{p}_t(k)-\boldsymbol{p}_r(k)\|_2^2}\right)\right], \tag{19}$$

$$^{\dot{p}_t}U_{r,t,g}(k)=-\frac{f_c}{\mathrm{c}}[(A_{t,g}(k)-A_{t,r}(k))(B_{t,g}(k)-B_{t,r}(k))], \tag{20}$$

$$A_{t,g}(k)=\frac{x_t(k)-x_g(k)}{\|\boldsymbol{p}_g(k)-\boldsymbol{p}_t(k)\|_2}, \tag{21}$$

$$A_{t,r}(k)=\frac{x_t(k)-x_r(k)}{\|\boldsymbol{p}_t(k)-\boldsymbol{p}_r(k)\|_2}, \tag{22}$$

$$B_{t,g}(k)=\frac{y_t(k)-y_g(k)}{\|\boldsymbol{p}_g(k)-\boldsymbol{p}_t(k)\|_2}, \tag{23}$$

$$B_{t,r}(k)=\frac{y_t(k)-y_r(k)}{\|\boldsymbol{p}_t(k)-\boldsymbol{p}_r(k)\|_2}, \tag{24}$$

$$^{x}\Omega_{t,g}(k)=\|\boldsymbol{p}_g(k)-\boldsymbol{p}_t(k)\|_2[\dot{x}_t(k)-\dot{x}_g(k)], \tag{25}$$

$$^{x}\Omega_{t,r}(k)=\|\boldsymbol{p}_t(k)-\boldsymbol{p}_r(k)\|_2[\dot{x}_t(k)-\dot{x}_r(k)], \tag{26}$$

$$^{y}\Omega_{t,g}(k)=\|\boldsymbol{p}_g(k)-\boldsymbol{p}_t(k)\|_2[\dot{y}_t(k)-\dot{y}_g(k)], \tag{27}$$

$$^{y}\Omega_{t,r}(k)=\|\boldsymbol{p}_t(k)-\boldsymbol{p}_r(k)\|_2[\dot{y}_t(k)-\dot{y}_r(k)], \tag{28}$$

$$\delta_{g,t}^{A}(k)=[\boldsymbol{p}_g(k)-\boldsymbol{p}_t(k)]^{\mathrm{T}}\cdot[\dot{\boldsymbol{p}}_g(k)-\dot{\boldsymbol{p}}_t(k)]A_{t,g}(k), \tag{29}$$

$$\delta_{t,r}^{A}(k)=[\boldsymbol{p}_t(k)-\boldsymbol{p}_r(k)]^{\mathrm{T}}\cdot[\dot{\boldsymbol{p}}_t(k)-\dot{\boldsymbol{p}}_r(k)]A_{t,r}(k), \tag{30}$$

$$\delta_{g,t}^{B}(k)=[\boldsymbol{p}_g(k)-\boldsymbol{p}_t(k)]^{\mathrm{T}}\cdot[\dot{\boldsymbol{p}}_g(k)-\dot{\boldsymbol{p}}_t(k)]B_{t,g}(k), \tag{31}$$

$$\delta_{t,r}^{B}(k)=[\boldsymbol{p}_t(k)-\boldsymbol{p}_r(k)]^{\mathrm{T}}\cdot[\dot{\boldsymbol{p}}_t(k)-\dot{\boldsymbol{p}}_r(k)]B_{t,r}(k), \tag{32}$$

$$^{p_g}O_{r,t,g}(k)=-\frac{f_c}{\mathrm{c}}\left[\left(\frac{^{x}\Omega_{g,r}(k)-\delta_{r,g}^{C}(k)}{\|\boldsymbol{p}_r(k)-\boldsymbol{p}_g(k)\|_2^2}+\frac{^{x}\Omega_{g,t}(k)-\delta_{g,t}^{C}(k)}{\|\boldsymbol{p}_g(k)-\boldsymbol{p}_t(k)\|_2^2}\right),\left(\frac{^{y}\Omega_{g,r}(k)-\delta_{r,g}^{D}(k)}{\|\boldsymbol{p}_r(k)-\boldsymbol{p}_g(k)\|_2^2}+\frac{^{y}\Omega_{g,t}(k)-\delta_{g,t}^{D}(k)}{\|\boldsymbol{p}_g(k)-\boldsymbol{p}_t(k)\|_2^2}\right)\right], \tag{33}$$

$$^{\dot{p}_g}O_{r,t,g}(k)=-\frac{f_c}{\mathrm{c}}[(C_{g,r}(k)+C_{g,t}(k))\cdot(D_{g,r}(k)+D_{g,t}(k))], \tag{34}$$

$$C_{g,r}(k)=\frac{x_g(k)-x_r(k)}{\|\boldsymbol{p}_r(k)-\boldsymbol{p}_g(k)\|_2}, \tag{35}$$

$$C_{g,t}(k)=\frac{x_g(k)-x_t(k)}{\|\boldsymbol{p}_g(k)-\boldsymbol{p}_t(k)\|_2}, \tag{36}$$

$$D_{g,r}(k)=\frac{y_g(k)-y_r(k)}{\|\boldsymbol{p}_r(k)-\boldsymbol{p}_g(k)\|_2}, \tag{37}$$

$$D_{g,t}(k)=\frac{y_g(k)-y_t(k)}{\|\boldsymbol{p}_g(k)-\boldsymbol{p}_t(k)\|_2}, \tag{38}$$

$$^{x}\Omega_{g,r}(k)=\|\boldsymbol{p}_r(k)-\boldsymbol{p}_g(k)\|_2[\dot{x}_g(k)-\dot{x}_r(k)], \tag{39}$$

$$^{x}\Omega_{g,t}(k)=\|\boldsymbol{p}_g(k)-\boldsymbol{p}_t(k)\|_2[\dot{x}_g(k)-\dot{x}_t(k)], \tag{40}$$

$$^{y}\Omega_{g,r}(k)=\|\boldsymbol{p}_r(k)-\boldsymbol{p}_g(k)\|_2[\dot{y}_g(k)-\dot{y}_r(k)], \tag{41}$$

$$^{y}\Omega_{g,t}(k)=\|\boldsymbol{p}_g(k)-\boldsymbol{p}_t(k)\|_2[\dot{y}_g(k)-\dot{y}_t(k)], \tag{42}$$

$$\delta_{r,g}^{C}(k)=[\boldsymbol{p}_r(k)-\boldsymbol{p}_g(k)]^{\mathrm{T}}\cdot[\dot{\boldsymbol{p}}_r(k)-\dot{\boldsymbol{p}}_g(k)]C_{g,r}(k), \tag{43}$$

$$\delta_{g,t}^{C}(k)=[\boldsymbol{p}_g(k)-\boldsymbol{p}_t(k)]^{\mathrm{T}}\cdot[\dot{\boldsymbol{p}}_g(k)-\dot{\boldsymbol{p}}_t(k)]C_{g,t}(k), \tag{44}$$

$$\delta_{r,g}^{D}(k)=[\boldsymbol{p}_r(k)-\boldsymbol{p}_g(k)]^{\mathrm{T}}\cdot[\dot{\boldsymbol{p}}_r(k)-\dot{\boldsymbol{p}}_g(k)]D_{g,r}(k), \tag{45}$$

$$\delta_{g,t}^{D}(k)=[\boldsymbol{p}_g(k)-\boldsymbol{p}_t(k)]^{\mathrm{T}}\cdot[\dot{\boldsymbol{p}}_g(k)-\dot{\boldsymbol{p}}_t(k)]D_{g,t}(k). \tag{46}$$

Hence, based on (17), $\mathrm{rank}[\boldsymbol{\Gamma}_L(0,l)]=8$, $\forall l\geqslant4$. In particular, when $l=1$, the rank of $\boldsymbol{\Gamma}_L(0,l)$ is 5 with linearly independent rows 1, 2, 3, 4, and 6. Both the rank and the number of linearly independent rows increase by one as each additional time step adds until $l=4$. Finally, all the linearly independent rows are 1, 2, 3, 4, 6, 12, 18, and 24. Therefore, the system is proved to be locally observable.

(ii) Analysis with JOT. For the nonlinear observability test, the only linearly independent rows are $\{\nabla_{\boldsymbol{X}}^{\mathrm{T}}[L_{f_0}^0\boldsymbol{h}_q(\boldsymbol{X})], q=1,2,3,4;\ \nabla_{\boldsymbol{X}}^{\mathrm{T}}[L_{f_0}^p\boldsymbol{h}_q(\boldsymbol{X})], p=0,1,q=6,7\}$ in terms of the matrix $\boldsymbol{\Gamma}_{NL}$. Hence, $\mathrm{rank}(\boldsymbol{\Gamma}_{NL})=8$.

For the linear observability test, the Jacobian matrix with the corresponding observation vector $\boldsymbol{Z}_o$ is

$$\boldsymbol{H}(k)=\begin{bmatrix}\boldsymbol{I}_{4\times4} & \boldsymbol{0}\\ \boldsymbol{\zeta}_{r,t}(k) & \boldsymbol{0}\\ \boldsymbol{S}_{r,g,t}(k) & \boldsymbol{V}_{r,g,t}(k)\\ \boldsymbol{0} & \boldsymbol{\psi}_{r,g}(k)\end{bmatrix} \tag{47}$$

where

$$\boldsymbol{\psi}_{r,g}(k)=[-D_{g,r}(k),C_{g,r}(k),0,0], \tag{48}$$

$$\boldsymbol{S}_{r,g,t}(k)=[A_{t,g}(k),B_{t,g}(k),0,0], \tag{49}$$

$$\boldsymbol{V}_{r,g,t}(k)=[(C_{g,r}(k)+C_{g,t}(k)),(D_{g,r}(k)+D_{g,t}(k)),0,0]. \tag{50}$$

Based on (17), $\mathrm{rank}[\boldsymbol{\Gamma}_L(0,l)]=8,\ \forall l\geqslant 2$. In particular, the rank of $\boldsymbol{\Gamma}_L(0,l)$ is 6 at the first time step, where rows 1, 2, 3, 4, 6, and 7 are linearly uncorrelated. When $l=2$, the rank of $\boldsymbol{\Gamma}_L(0,l)$ increases to 8 with additional linearly independent rows 13 and 14, and will no longer increase as the time step increases.

Consider the collinear geometry case. More simply, the target is assumed to locate between the IO and the receiver, i.e., $x_g>x_r$ and $y_g>y_r$. Hence, the system measurements have the following relationship: $\alpha(k)=\beta(k)$, $f_d(k)=0$, and $\rho(k)=\|\boldsymbol{p}_r(k)-\boldsymbol{p}_t(k)\|_2$. Therefore, the ranks of observability matrices $\boldsymbol{\Gamma}_{NL}$ and $\boldsymbol{\Gamma}_L$ all drop to 4 for both SOT and JOT cases. Besides, no observable states exist in the null space of the corresponding observability matrix except the known IO states [26].

3.2.2 Observability analysis

The forthcoming analysis will give the theorems and proofs about the system observability.

Theorem 1 In the SRSTSIO scenario with unknown IO states, the passive radar system is observable for both SOT and JOT cases.

Proof The system state vector in this case is defined as $\boldsymbol{X}=[\boldsymbol{X}_t^{\mathrm{T}},\boldsymbol{X}_g^{\mathrm{T}}]^{\mathrm{T}}$, where the corresponding state transition matrix is $\boldsymbol{F}=\mathrm{diag}[\boldsymbol{F}_t,\boldsymbol{F}_g]$. The observation vector is $\boldsymbol{Z}_s=[\alpha,f_d]^{\mathrm{T}}$ for SOT, and $\boldsymbol{Z}_o=[\alpha,\rho,\beta]^{\mathrm{T}}$ for JOT.

(i) Analysis with SOT. For the nonlinear observability test, rows $\left\{\nabla_{\boldsymbol{X}}^{\mathrm{T}}[L_{f_0}^p\boldsymbol{h}_1(\boldsymbol{X})],\ p=0,1,2;\ \nabla_{\boldsymbol{X}}^{\mathrm{T}}[L_{f_0}^p\boldsymbol{h}_2(\boldsymbol{X})],\ p=0,1,\cdots,4\right\}$ are linearly uncorrelated in terms of the matrix $\boldsymbol{\Gamma}_{NL}$. Hence, $\mathrm{rank}(\boldsymbol{\Gamma}_{NL})=8$.

For the linear observability test, empty knowledge of IO initial states yields the Jacobian matrix given as

$$\boldsymbol{H}(k)=\begin{bmatrix}\boldsymbol{\zeta}_{r,t}(k) & \boldsymbol{0}\\ \boldsymbol{U}_{r,t,g}(k) & \boldsymbol{O}_{r,t,g}(k)\end{bmatrix}. \tag{51}$$

Hence, based on (17), $\mathrm{rank}[\boldsymbol{\Gamma}_L(0,l)]=8,\ \forall l\geqslant 5$. In particular, when $l=1$, the rank of $\boldsymbol{\Gamma}_L(0,l)$ is 2 with linearly independent rows 1 and 2. The rank increases by 2 as each additional time step adds until $l=3$. The corresponding additional linearly independent rows are 3 and 4 at $l=2$, and 5 and 6 at $l=3$. The rank increases to 7 with additional linearly independent row 8 at $l=4$. When $l=5$, the rank increases to 8 and will no longer increase as the time step increases. Finally, rows 1, 2, 3, 4, 5, 6, 8, and 10 are all linearly uncorrelated.

(ii) Analysis with JOT. For the nonlinear observability test, rows $\left\{\nabla_{\boldsymbol{X}}^{\mathrm{T}}[L_{f_0}^p\boldsymbol{h}_q(\boldsymbol{X})], p=0,1,q=1,2,3;\ \nabla_{\boldsymbol{X}}^{\mathrm{T}}[L_{f_0}^2\boldsymbol{h}_q(\boldsymbol{X})], q=1,2\right\}$ are linearly uncorrelated in terms of the matrix $\boldsymbol{\Gamma}_{NL}$. Hence, $\mathrm{rank}(\boldsymbol{\Gamma}_{NL})=8$.

For the linear observability test, the Jacobian matrix is

$$\boldsymbol{H}(k)=\begin{bmatrix}\boldsymbol{\zeta}_{r,t}(k) & \boldsymbol{0}\\ \boldsymbol{S}_{r,g,t}(k) & \boldsymbol{V}_{r,g,t}(k)\\ \boldsymbol{0} & \boldsymbol{\psi}_{r,g}(k)\end{bmatrix}. \tag{52}$$

Hence, based on (17), $\mathrm{rank}[\boldsymbol{\Gamma}_L(0,l)]=8,\ \forall l\geqslant 3$. In particular, when $l=1$, the rank of $\boldsymbol{\Gamma}_L(0,l)$ is 3 with linearly independent rows 1, 2, and 3. The rank increases to 6 at $l=2$. Three additional linearly independent rows 4, 5, and 6 are added. When $l=3$, the rank increases to 8 and will no longer increase as the time step increases. Finally, the linearly independent rows are from 1 to 8. □

Theorem 2 In the SRMTSIO scenario with unknown IO states, the passive radar system is observable for both SOT and JOT cases.

Proof The system sate vector in this case is defined as $\boldsymbol{X}=[\boldsymbol{X}_t^{\mathrm{T}},\boldsymbol{X}_{g_1}^{\mathrm{T}},\boldsymbol{X}_{g_2}^{\mathrm{T}},\cdots,\boldsymbol{X}_{g_N}^{\mathrm{T}}]^{\mathrm{T}}$, where the corresponding state transition matrix is $\boldsymbol{F}=\mathrm{diag}[\boldsymbol{F}_t,\boldsymbol{F}_{g_1},\boldsymbol{F}_{g_2},\cdots,\boldsymbol{F}_{g_N}]$. The observation vector is $\boldsymbol{Z}_s=[\alpha,f_{d_1},f_{d_2},\cdots,f_{d_N}]^{\mathrm{T}}$ for SOT, and $\boldsymbol{Z}_o=[\alpha,\rho_1,\beta_1,\rho_2,\beta_2,\cdots,\rho_N,\beta_N]^{\mathrm{T}}$ for JOT.

(i) Analysis with SOT. For the nonlinear observability test, the results are identical to Theorem 1 for $N=1$. For $N\geqslant 2$, the only linearly independent rows are $\left\{\nabla_{\boldsymbol{X}}^{\mathrm{T}}[L_{f_0}^p\boldsymbol{h}_1(\boldsymbol{X})], p=0,1,2;\ \nabla_{\boldsymbol{X}}^{\mathrm{T}}[L_{f_0}^p\boldsymbol{h}_2(\boldsymbol{X})], p=0,1,2,3,4;\ \nabla_{\boldsymbol{X}}^{\mathrm{T}}[L_{f_0}^p\boldsymbol{h}_2(\boldsymbol{X})], p=0,1,2,3, q=3,4,\cdots,N+1\right\}$ according to the matrix $\boldsymbol{\Gamma}_{NL}$. Hence, $\mathrm{rank}(\boldsymbol{\Gamma}_{NL})=4N+4$.

For the linear observability test, the Jacobian matrix is

$$\boldsymbol{H}(k)=\begin{bmatrix}\boldsymbol{\zeta}_{r,t}(k) & \boldsymbol{0} & \cdots & \boldsymbol{0}\\ \boldsymbol{U}_{r,t,g_1}(k) & \boldsymbol{O}_{r,t,g_1}(k) & \cdots & \boldsymbol{0}\\ \vdots & \vdots & \ddots & \vdots\\ \boldsymbol{U}_{r,t,g_N}(k) & \boldsymbol{0} & \cdots & \boldsymbol{O}_{r,t,g_N}(k)\end{bmatrix}. \tag{53}$$

Hence, $\text{rank}[\boldsymbol{\Gamma}_L(0,l)]=4N+4,\ \forall l\geqslant 5$ for $N\geqslant 1$. In particular, when $l=1$, the rank of $\boldsymbol{\Gamma}_L(0,l)$ is $N+1$ with linearly independent rows $1,2,\cdots,N+1$. The rank doubles as each additional time step adds until $l=3$, all the linearly independent rows of which are from 1 to $3N+3$. The rank increases to $4N+3$ with additional linearly independent rows $3N+5$, $3N+6$, $\cdots$, $4N+4$ at $l=4$. When $l=5$, the rank increases to $4N+4$ and will no longer increase as the time step increases. Finally, the additional linearly independent row $4N+6$ is added.

(ii) Analysis with JOT. For the nonlinear observability test, rows $\{\nabla_{\boldsymbol{X}}^{\mathrm{T}}[L_{f_0}^p\boldsymbol{h}_q(\boldsymbol{X})],p=0,1,\ q=1,2,\cdots,2N+1;\ \nabla_{\boldsymbol{X}}^{\mathrm{T}}[L_{f_0}^2\boldsymbol{h}_q(\boldsymbol{X})],q=1,2\}$ are linearly uncorrelated in terms of the matrix $\boldsymbol{\Gamma}_{NL}$ for $N\geqslant 1$. Hence, $\text{rank}(\boldsymbol{\Gamma}_{NL})=4N+4$.

For the linear observability test, the Jacobian matrix is

$$\boldsymbol{H}(k)=\begin{bmatrix}\boldsymbol{\zeta}_{r,t}(k) & \boldsymbol{0} & \cdots & \boldsymbol{0}\\ \boldsymbol{S}_{r,g_1,t}(k) & \boldsymbol{V}_{r,g_1,t}(k) & \cdots & \boldsymbol{0}\\ \boldsymbol{0} & \boldsymbol{\psi}_{r,g_1}(k) & \cdots & \boldsymbol{0}\\ \vdots & \vdots & \ddots & \vdots\\ \boldsymbol{S}_{r,g_N,t}(k) & \boldsymbol{0} & \cdots & \boldsymbol{V}_{r,g_N,t}(k)\\ \boldsymbol{0} & \boldsymbol{0} & \cdots & \boldsymbol{\psi}_{r,g_N}(k)\end{bmatrix}. \tag{54}$$

Based on (17), for $N\geqslant 1$, $\text{rank}[\boldsymbol{\Gamma}_L(0,l)]=4N+4$, $\forall l\geqslant 3$. In particular, when $l=1$, the rank of $\boldsymbol{\Gamma}_L(0,l)$ is $2N+1$ with linearly independent rows from 1 to $2N+1$. The rank doubles at $l=2$, all the linearly independent rows of which are from 1 to $4N+2$. When $l=3$, the rank increases to $4N+4$ and will no longer increase as the time step increases. Finally, all the linearly independent rows are from 1 to $4N+4$. □

Theorem 3 In the SRSTMIOs scenario with unknown IO states, the passive radar system is observable for both SOT and JOT cases.

Proof The system state vector in this case is defined as $\boldsymbol{X}=[\boldsymbol{X}_{t_1}^{\mathrm{T}},\boldsymbol{X}_{t_2}^{\mathrm{T}},\cdots,\boldsymbol{X}_{t_M}^{\mathrm{T}},\boldsymbol{X}_g^{\mathrm{T}}]^{\mathrm{T}}$, where the corresponding state transition matrix is $\boldsymbol{F}=\text{diag}[\boldsymbol{F}_{t_1},\boldsymbol{F}_{t_2},\cdots,\boldsymbol{F}_{t_M},\boldsymbol{F}_g]$. The observation vector is $\boldsymbol{Z}_s=[\alpha_1,\cdots,\alpha_M,f_{d_1},\cdots,f_{d_M}]^{\mathrm{T}}$ for SOT, and $\boldsymbol{Z}_o=[\alpha_1,\cdots,\alpha_M,\rho_1,\cdots,\rho_M,\beta]^{\mathrm{T}}$ for JOT.

(i) Analysis with SOT. For the nonlinear observability test, the results are identical to Theorem 1 for $M=1$. When $M\geqslant 2$, rows $\left\{\nabla_{\boldsymbol{X}}^{\mathrm{T}}[L_{f_0}^p\boldsymbol{h}_q(\boldsymbol{X})],p=0,1,q=1,2,\cdots,2M;\nabla_{\boldsymbol{X}}^{\mathrm{T}}[L_{f_0}^2\boldsymbol{h}_q(\boldsymbol{X})],\ q=1,2,3,4\right\}$ are linearly uncorrelated according to the nonlinear observability matrix $\boldsymbol{\Gamma}_{NL}$. Hence, $\text{rank}(\boldsymbol{\Gamma}_{NL})=4M+4$.

For the linear observability test, the Jacobian matrix is

$$\boldsymbol{H}(k)=\begin{bmatrix}\boldsymbol{\zeta}_{r,t_1}(k) & \boldsymbol{0} & \boldsymbol{0} & \cdots & \boldsymbol{0}\\ \boldsymbol{0} & \boldsymbol{\zeta}_{r,t_2}(k) & \boldsymbol{0} & \cdots & \boldsymbol{0}\\ \vdots & \vdots & \vdots & \ddots & \vdots\\ \boldsymbol{0} & \boldsymbol{0} & \cdots & \boldsymbol{\zeta}_{r,t_M}(k) & \boldsymbol{0}\\ \boldsymbol{U}_{r,t_1,g}(k) & \boldsymbol{0} & \boldsymbol{0} & \cdots & \boldsymbol{O}_{r,t_1,g}(k)\\ \boldsymbol{0} & \boldsymbol{U}_{r,t_2,g}(k) & \boldsymbol{0} & \cdots & \boldsymbol{O}_{r,t_2,g}(k)\\ \vdots & \vdots & \vdots & \ddots & \vdots\\ \boldsymbol{0} & \boldsymbol{0} & \cdots & \boldsymbol{U}_{r,t_M,g}(k) & \boldsymbol{O}_{r,t_M,g}(k)\end{bmatrix}. \tag{55}$$

Based on (17), for $M=1$, the results are identical to Theorem 1, where the matrix $\boldsymbol{\Gamma}_L(0,l)$ is full rank when the time step is at least 5. For $M\geqslant 2$, $\text{rank}[\boldsymbol{\Gamma}_L(0,l)]=4M+4$, $\forall l\geqslant 3$. In particular, the rank of $\boldsymbol{\Gamma}_L(0,l)$ is $2M$ at $l=1$ with linearly independent rows from 1 to $2M$. The rank doubles at $l=2$, all the linearly independent rows of which are from 1 to $4M$. When $l=3$, the rank increases to $4M+4$ and will no longer increase as the time step increases. Finally, all the linearly independent rows are from 1 to $4M+4$.

(ii) Analysis with JOT. For the nonlinear observability test, the results are identical to Theorem 1 for $M=1$. When $M=2$, rows $\left\{\nabla_{\boldsymbol{X}}^{\mathrm{T}}[L_{f_0}^p\boldsymbol{h}_1(\boldsymbol{X})],\ p=0,2;\nabla_{\boldsymbol{X}}^{\mathrm{T}}[L_{f_0}^p\boldsymbol{h}_q(\boldsymbol{X})],p=0,1,q=2,3,4,5;\ \nabla_{\boldsymbol{X}}^{\mathrm{T}}[L_{f_0}^2\boldsymbol{h}_q(\boldsymbol{X})],\ q=3,4\right\}$ are linearly uncorrelated. For $M\geqslant 3$, if M is odd, rows $\left\{\nabla_{\boldsymbol{X}}^{\mathrm{T}}[L_{f_0}^0\boldsymbol{h}_q(\boldsymbol{X})],\ q=1,2,\cdots,M+3,M+5,\cdots,2M;\ \nabla_{\boldsymbol{X}}^{\mathrm{T}}[L_{f_0}^1\boldsymbol{h}_q(\boldsymbol{X})],\ q=1,3,\cdots,M,M+1,\cdots,2M+1;\ \nabla_{\boldsymbol{X}}^{\mathrm{T}}[L_{f_0}^2\boldsymbol{h}_q(\boldsymbol{X})],q=1,3,\cdots,2M-1,2M\right\}$ are linearly uncorrelated. Whereas, if M is even, rows $\left\{\nabla_{\boldsymbol{X}}^{\mathrm{T}}[L_{f_0}^0\boldsymbol{h}_q(\boldsymbol{X})],q=1,2,\cdots,M+3,M+5,\cdots,2M+1;\ \nabla_{\boldsymbol{X}}^{\mathrm{T}}[L_{f_0}^1\boldsymbol{h}_q(\boldsymbol{X})],q=2,4,\cdots,M,M+1,\cdots,2M+1;\ \nabla_{\boldsymbol{X}}^{\mathrm{T}}[L_{f_0}^2\boldsymbol{h}_q(\boldsymbol{X})],q=1,3,\cdots,2M-1,2M\right\}$ are linearly uncorrelated. Hence, $\text{rank}(\boldsymbol{\Gamma}_{NL})=4M+4$.

For the linear observability test, the Jacobian matrix is

$$\boldsymbol{H}(k)=\begin{bmatrix}\boldsymbol{\zeta}_{r,t_1}(k) & \boldsymbol{0} & \boldsymbol{0} & \cdots & \boldsymbol{0}\\ \boldsymbol{0} & \boldsymbol{\zeta}_{r,t_2}(k) & \boldsymbol{0} & \cdots & \boldsymbol{0}\\ \vdots & \vdots & \vdots & \ddots & \vdots\\ \boldsymbol{0} & \boldsymbol{0} & \cdots & \boldsymbol{\zeta}_{r,t_M}(k) & \boldsymbol{0}\\ \boldsymbol{S}_{r,g,t_1}(k) & \boldsymbol{0} & \boldsymbol{0} & \cdots & \boldsymbol{V}_{r,g,t_1}(k)\\ \boldsymbol{0} & \boldsymbol{0} & \boldsymbol{0} & \cdots & \boldsymbol{\psi}_{r,g}(k)\\ \boldsymbol{0} & \boldsymbol{S}_{r,g,t_2}(k) & \boldsymbol{0} & \cdots & \boldsymbol{V}_{r,g,t_2}(k)\\ \vdots & \vdots & \vdots & \ddots & \vdots\\ \boldsymbol{0} & \boldsymbol{0} & \cdots & \boldsymbol{S}_{r,g,t_M}(k) & \boldsymbol{V}_{r,g,t_M}(k)\end{bmatrix}. \tag{56}$$

Based on (17), $\text{rank}[\boldsymbol{\Gamma}_L(0,l)]=4N+4$, $\forall l\geqslant 3$. In particular, for $1\leqslant M\leqslant 2$, the rank of $\boldsymbol{\Gamma}_L(0,l)$ is $2M+1$ at $l=1$ with linearly independent rows from 1 to $2M+1$. The rank increases to $4M+2$, where additional linearly

independent rows $3M+1$, $3M+2,\cdots$, $5M+1$ are added. When $l=3$, the rank increases to $4M+4$ and will no longer increase as the time step increases. Additional linearly independent rows $6M+1$ and $6M+2$ are added. If $M\geqslant 3$, the rank of $\boldsymbol{\Gamma}_L(0,l)$ is $2M+1$ at $l=1$, where rows $1,2,\cdots,M+3,M+5,\cdots,3M-1$ are linearly independent. The rank increases to $4M+2$ with additional linearly independent rows $3M+1,3M+2,\cdots,4M+3,4M+5,\cdots,6M-1$ at $l=2$. When $l=3$, the rank increases to $4M+4$ and will no longer increase as the time step increases. Additional linearly independent rows $6M+1$ and $6M+2$ are added. □

From Theorems 1−3, one can see that passive radar systems with unknown IO states in these three scenarios are all observable for both SOT and JOT cases. It is also obvious that both linear and nonlinear observability tests are applicable to these systems. Besides, for the linear observability test, the length of time steps to make the observability matrix full rank with JOT is generally less than that with SOT. Moreover, adding the number of IOs can diminish the length of time steps to make the observability matrix full rank for SOT. Without loss of generality, our method can also analyze the scenario including multiple receivers with multiple IOs and targets.

4. Estimablity analysis

The observability can only qualitatively but not quantitatively reflect the characteristics of the system. However, the degree of observability, i.e., estimability, also needs to be considered. The estimability can assess whether the system has good or poor observability. Herein, the method in [40] is adopted, where the estimability of different states of the system is assessed by decomposing the normalized error covariance matrix of the filter. The purposes of the normalization are twofold: (i) transforming the estimation error covariance matrix to be dimensionless, and (ii) bounding the eigenvalues between zero and n. The first purpose is based on a congruent transformation given as follows:

$$\boldsymbol{P}'(k+1)=[\sqrt{\boldsymbol{P}(0)}]^{-1}\boldsymbol{P}(k+1)[\sqrt{\boldsymbol{P}(0)}]^{-1} \tag{57}$$

where $\boldsymbol{P}(0)$ is the initial estimation error covariance, $\boldsymbol{P}(k+1)$ is the posterior estimation error covariance, and $\boldsymbol{P}'(k+1)$ is the modified version of $\boldsymbol{P}(k+1)$. Here, $\boldsymbol{P}(0)$ is assumed to be diagonal and positive definite. This transformation makes the comparisons between the eigenvalues meaningful. The other purpose is achieved based on

$$\boldsymbol{P}''(k+1)=\frac{n}{\mathrm{trace}[\boldsymbol{P}'(k+1)]}\boldsymbol{P}'(k+1) \tag{58}$$

where $\boldsymbol{P}''(k+1)$ is the modified version of $\boldsymbol{P}'(k+1)$.

The eigenvalues and eigenvectors of $\boldsymbol{P}''(k+1)$ can reflect the characteristics of the system states. In particular, a large eigenvalue represents a low estimability, which means the linear combination of system states has poor observability. The corresponding eigenvector provides the direction of such low estimability. Whereas, the most observable linear combination of states is demonstrated by the smallest eigenvalues [41].

5. Simulation results

Herein, only the SRMTSIO and SRSTMIOs cases are tested. If the analysis results in this two cases are correct, then the analysis results in the SRSTSIO case are also correct. Note that all the observations are centrally processed in the EKF. If a system is observable, the corresponding estimation error covariance should be converged, and the estimation error $\Delta\boldsymbol{X}=\widehat{\boldsymbol{X}}-\boldsymbol{X}$ will remain bounded for a single-run EKF, where $\widehat{\boldsymbol{X}}$ is the EKF state estimation and $\boldsymbol{X}$ is the true state [41].

For the SRMTSIO case, two targets are considered, where the true initial states of the IO and targets with NCV models are assumed to be $\boldsymbol{X}_t(0)$, $\boldsymbol{X}_{g_1}(0)$, and $\boldsymbol{X}_{g_2}(0)$, respectively. The receiver maneuvers following the coordinated turn model with respect to the initial state $\boldsymbol{X}_r(0)$, where the turn rate is $\frac{1.2\pi}{180}$ rad/s. Assume that both the IO and targets have the same initial estimation error covariance $\boldsymbol{P}_t(0)$ and process noise covariance $\boldsymbol{Q}_t(0)$, where

$$\boldsymbol{Q}_t(0)=\begin{bmatrix}1\times10^{-3}&0&1\times10^{-3}&0\\0&2.5\times10^{-4}&0&5\times10^{-4}\\1\times10^{-3}&0&1\times10^{-3}&0\\0&5\times10^{-4}&0&1\times10^{-3}\end{bmatrix}. \tag{59}$$

The carrier frequency of the IO is 6 GHz. Suppose that the IO and targets have the same initial estimation error, i.e., $\Delta\boldsymbol{X}_t(0)=\Delta\boldsymbol{X}_g(0)$. The specific simulation parameter settings are listed in Table 1.

Table 1 Simulation parameter settings for SRMTSIO case

Parameter	Value
$\boldsymbol{X}_t(0)$	$[52\,000, 30\,000, -50\sqrt{2}, 50\sqrt{2}]^{\mathrm{T}}$
$\boldsymbol{X}_{g_1}(0)$	$[45\,000, -10\,000, -40, -40\sqrt{3}]^{\mathrm{T}}$
$\boldsymbol{X}_{g_2}(0)$	$[60\,000, -20\,000, -40, 40\sqrt{3}]^{\mathrm{T}}$
$\boldsymbol{X}_r(0)$	$[15\,000, 18\,000, -100, -100]^{\mathrm{T}}$
$\boldsymbol{P}_t(0)$	$\mathrm{diag}[3\,000^2, 3\,000^2, 100^2, 100^2]$
σ_α/rad	0.001
σ_β/rad	0.001
σ_α/Hz	0.001
σ_ρ/m	100
$\Delta\boldsymbol{X}_t(0)$	$[150, -150, 5, -5]^{\mathrm{T}}$
$\Delta\boldsymbol{X}_g(0)$	$[150, -150, 5, -5]^{\mathrm{T}}$

For the SRSTMIOs case, the additional IO with the initial state $\boldsymbol{X}_{t_2}(0) = [50\,000, 40\,000, 50\sqrt{2}, -50\sqrt{2}]^{\mathrm{T}}$ is assumed to exist based on the simulation settings in the SRMTSIO case. Simultaneously, the target with $\boldsymbol{X}_g(0) = [45\,000, -10\,000, -40, -40\sqrt{3}]^{\mathrm{T}}$ is retained. Other simulation settings remain the same as defined in the SRMTSIO case. The results for $\Delta\boldsymbol{X}_i$ associated with the estimation error variance bounds $\pm 2\sigma_i$ in the two cases are plotted in Fig. 1 and Fig. 2, where $i = 1, 2, \cdots, n$ represents the ith element of the system state $\boldsymbol{X}$. Fig. 3 and Fig. 4 demonstrate the corresponding results for the eigenvectors with regard to the largest and smallest eigenvalues based on the EKF, which gives the least and the most observable directions in the two scenarios, respectively. Specifically, the ith system state in Fig. 3 and Fig. 4 represents the ith element of the system state vectors defined in Theorem 2 and Theorem 3, respectively.

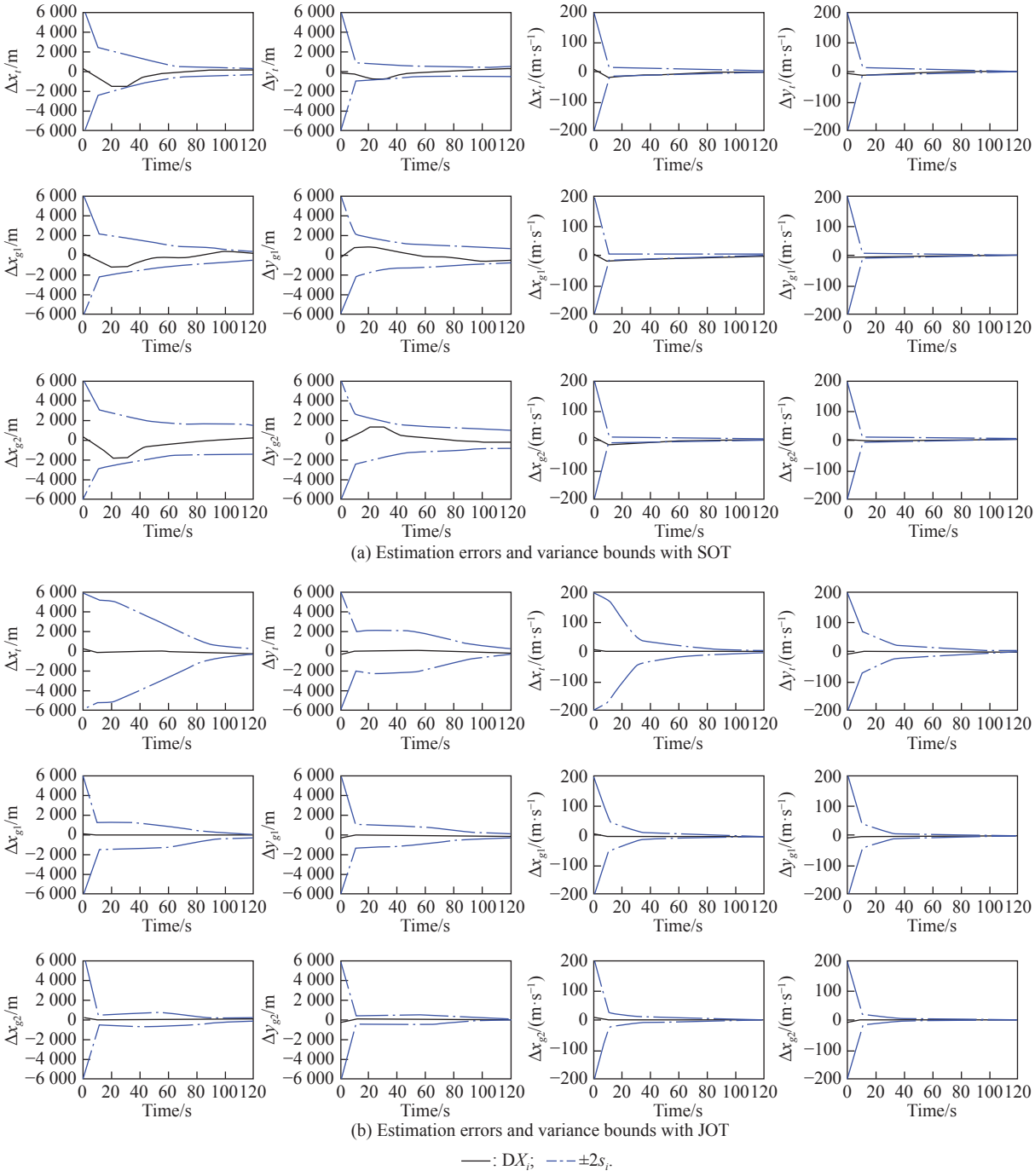

Fig. 1 Estimation errors and variance bounds for SRMTSIO case

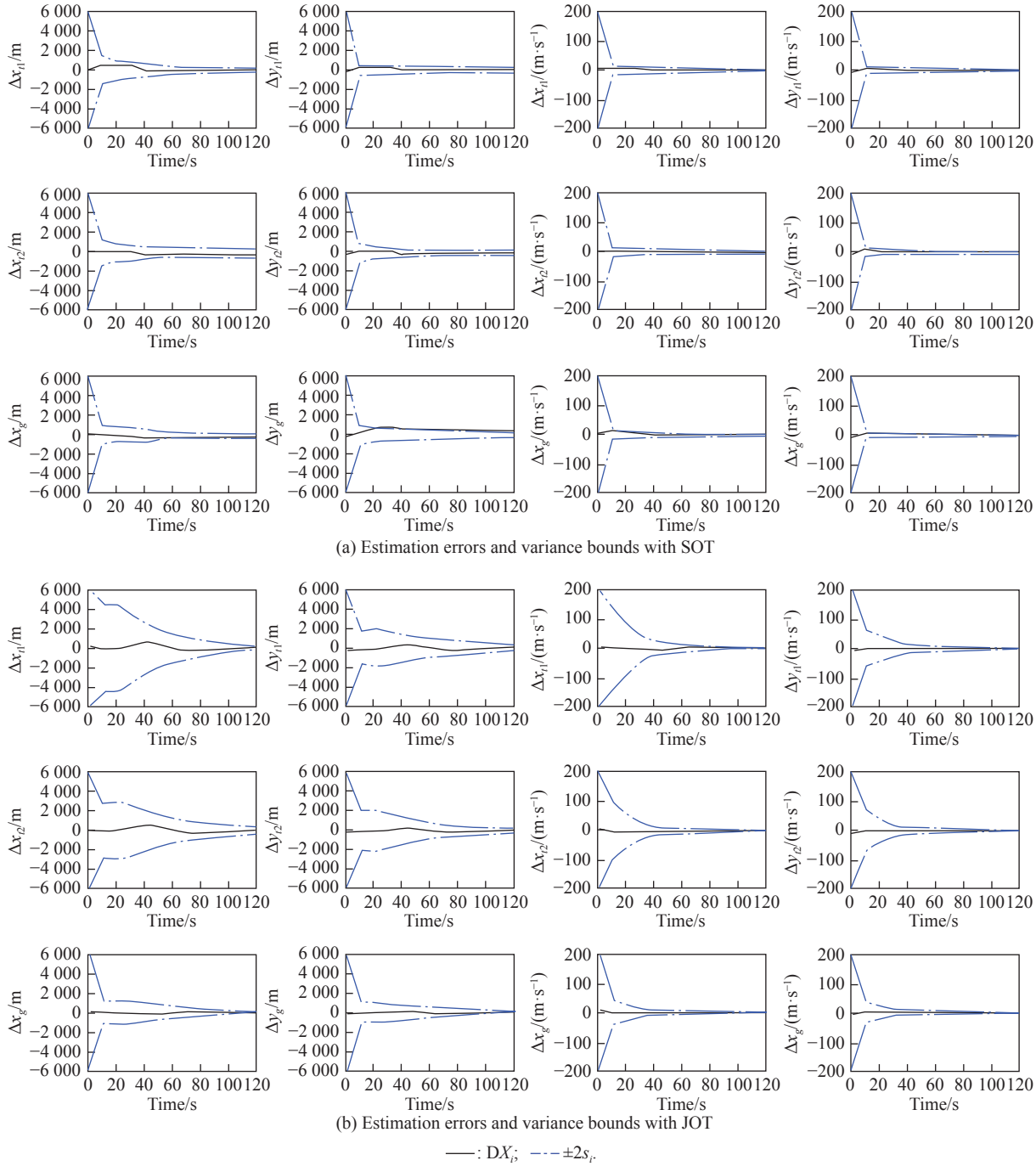

Fig. 2 Estimation errors and variance bounds for SRSTMIOs case

From Fig. 1 and Fig. 2, one can see that the estimation error variances converge, and the estimation errors remain bounded, which indicates that the systems with JOT and SOT are observable in each case, that is, confirming the correctness of the theoretical analysis. From Fig. 3, it can be concluded that, in the SRMTSIO scenario with JOT, the linear combination of the fifth, sixth, seventh, and eighth states of the system, in terms of x_{g_1}, y_{g_1}, $\dot{x}_{g_1}$ and $\dot{y}_{g_1}$, will have a high estimability, whereas the linear combination of the first, second, fifth, sixth, ninth, and tenth states, in terms of x_t, y_t, x_{g_1}, y_{g_1}, x_{g_2} and y_{g_2}, will have a low estimability according to the rest of the states. That is, the states of the first target could be better estimated. As for SOT, the linear combination of the third, eighth, eleventh, and twelfth states, in terms of $\dot{x}_t$, $\dot{y}_{g_1}$, $\dot{x}_{g_2}$ and $\dot{y}_{g_2}$, will have a high estimability, whereas the linear combination of the ninth and tenth states, in terms of x_{g_2} and y_{g_2}, will have a low estimability according to the rest of the sates.

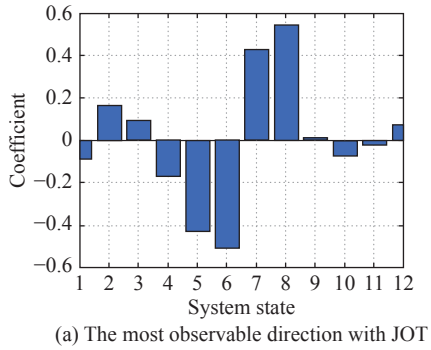

(a) The most observable direction with JOT

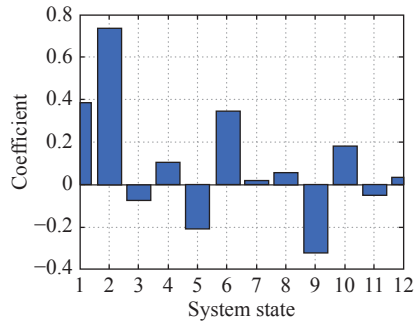

(b) The least observable direction with JOT

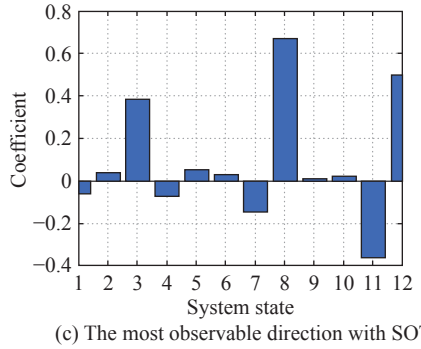

(c) The most observable direction with SOT

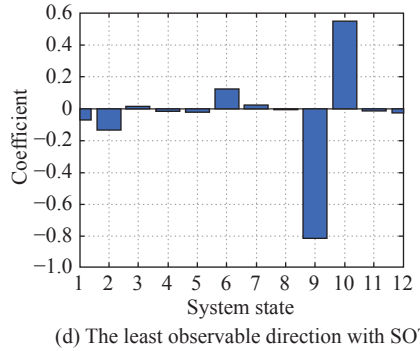

(d) The least observable direction with SOT

Fig. 3 The least and the most observable directions according to the system states for SRMTSIO case

Relatively speaking, the Doppler difference observation has an important effect on the velocity states. From Fig. 4, it is obvious that, in the SRSTMIOs scenario with JOT, the linear combination of the ninth, tenth, eleventh, and twelfth states, in terms of x_g, y_g, $\dot{x}_g$ and $\dot{y}_g$, will have a high estimability, whereas the linear combination of the first, second, fifth, sixth, ninth, and tenth states, in terms of x_{t_1}, y_{t_1}, x_{t_2}, y_{t_2}, x_g and y_g, will have a low estimability according to the rest of the states. As for SOT, the twelfth state, in terms of $\dot{y}_g$, will have a high estimability, whereas the linear combination of the fifth, sixth, and tenth states, in terms of x_{t_2}, y_{t_2}, x_g and y_g, will have a low estimability according to the rest of the states.

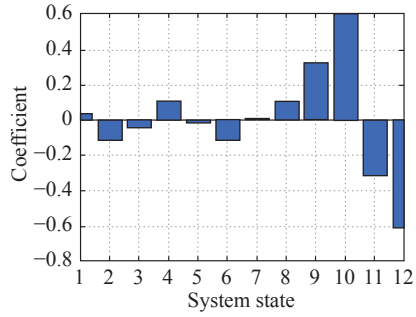

(a) The most observable direction with JOT

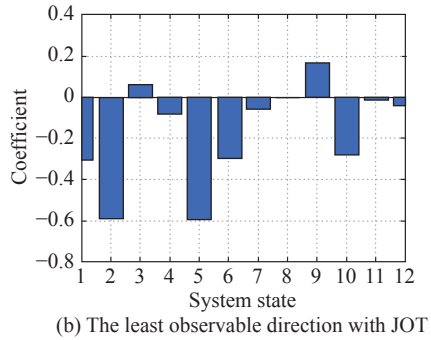

(b) The least observable direction with JOT

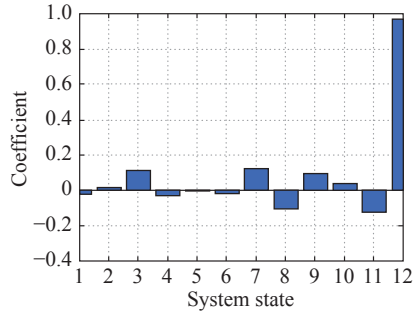

(c) The most observable direction with SOT

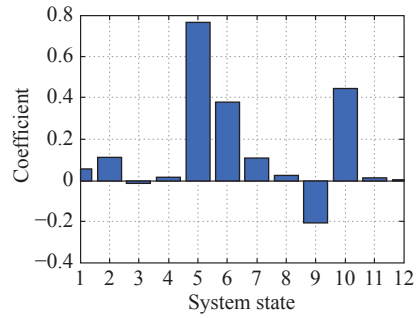

(d) The least observable direction with SOT

Fig. 4 The least and the most observable directions according to the system states for SRSTMIOs case

6. Conclusions

In this paper, we study the problem of observability and estimability analysis for passive radar systems with unknown IO states in three typical scenarios. Different observations are considered in each case. Linear and nonlinear observability tests are both considered to examine whether the system is observable. The estimability is also studied.

We observe that the systems in all scenarios are observable. The two observability tests that have the same conclusions are both applicable to the system. For the effect of different observations, the linear observability test with SOT generally needs more time steps to make the observability matrix full rank than that with JOT. Furthermore, increasing the number of IOs can decrease such time steps for SOT. Besides, the estimability, especially the directions of good and poor observability for the various states, is significantly dependent on the observations. In future work, we will consider the case, where the IOs and targets have various dynamic models.

References

[1] ZHANG X D, LI H B, HIMED B. Maximum likelihood delay and Doppler estimation for passive sensing. IEEE Sensors Journal, 2019, 19(1): 180–188.

[2] GOGINENI S, SETLUR P, RANGASWAMY M, et al. Passive radar detection with noisy reference channel using principal subspace similarity. IEEE Trans. on Aerospace and Electronic Systems, 2017, 54(1): 18–36.

[3] YI J X, WAN X R, LI D S, et al. Robust clutter rejection in passive radar via generalized subband cancellation. IEEE Trans. on Aerospace and Electronic Systems, 2018, 54(4): 1931–1946.

[4] GROMEK D, RADECKI K, DROZDOWICZ J, et al. Passive SAR imaging using DVB-T illumination for airborne applications. IET Radar, Sonar & Navigation, 2018, 13(2): 213–221.

[5] ZAIMBASHI A. Broadband target detection algorithm in FM-based passive bistatic radar systems. IET Radar, Sonar & Navigation, 2016, 10(8): 1485–1499.

[6] COLONE F, MARTELLI T, LOMBARDO P. Quasi-monostatic versus near forward scatter geometry in WiFi-based passive radar sensors. IEEE Sensors Journal, 2017, 17(15): 4757–4772.

[7] ZHANG X, LI H B, LIU J, et al. Joint delay and Doppler estimation for passive sensing with direct-path interference. IEEE Trans. on Signal Processing, 2016, 64(3): 630–640.

[8] WANG F Z, LI H B, ZHANG X, et al. Signal parameter estimation for passive bistatic radar with waveform correlation exploitation. IEEE Trans. on Aerospace and Electronic Systems, 2018, 54(3): 1135–1150.

[9] ABDULLAH R S A R, SALAH A A, ISMAIL A, et al. Experimental investigation on target detection and tracking in passive radar using long-term evolution signal. IET Radar, Sonar & Navigation, 2016, 10(3): 577–585.

[10] KASSAS Z M, HUMPHREYS T E. Receding horizon trajectory optimization in opportunistic navigation environments. IEEE Trans. on Aerospace and Electronic Systems, 2015, 51(2): 866–877.

[11] KALMAN R E. On the general theory of control systems. Proc. of the 1st International Conference on Automatic Control, 1960: 481–492.

[12] RAO S K. Comments on “Discrete-time observability and estimability analysis for bearings-only target motion analysis”. IEEE Trans. on Aerospace and Electronic Systems, 1998, 34(4): 1361–1367.

[13] GAD A S, MOJICA F, FAROOQ M. Geometric approach to target tracking motion analysis in bearing-only tracking. Proc. of SPIE: Signal Processing, Sensor Fusion, and Target Recognition XI, 2002, 4729: 1–12.

[14] JAUFFRET C, PILLON D. Observability in passive target motion analysis. IEEE Trans. on Aerospace and Electronic Systems, 1996, 32(4): 1290–1300.

[15] BECKER K. Simple linear theory approach to TMA observability. IEEE Trans. on Aerospace and Electronic Systems, 1993, 29(2): 575–578.

[16] SONG T L. Observability of target tracking with bearings-only measurements. IEEE Trans. on Aerospace and Electronic Systems, 1996, 32(4): 1468–1472.

[17] LEE T S, DUNN K P, CHANF C B. On observability and unbiased estimation of nonlinear systems. DRENICK R F, KOZIN F, ed. System modeling and optimization. Berlin, Heidelberg: Springer, 1982: 258–266.

[18] LEE S M, JUNG J, KIM S, et al. DV-SLAM (dual-sensor-based vector-field SLAM) and observability analysis. IEEE Trans. on Industrial Electronics, 2014, 62(2): 1101–1112.

[19] JAUFFRET C. Observability and Fisher information matrix in nonlinear regression. IEEE Trans. on Aerospace and Electronic Systems, 2007, 43(2): 756–759.

[20] FANG X P, YAN W S, WANG Y T, et al. Observability analysis of underwater localization based on Fisher information matrix. Proc. of the 32nd Chinese Control Conference, 2013: 4866–4869.

[21] BAR-SHALOM Y, LI X R, KIRUBARAJAN T. Estimation with applications to tracking and navigation: theory algorithms and software. New York: Wiley, 2004.

[22] GOSHEN-MESKIN D, BAR-ITZHACK I Y. Observability analysis of piece-wise constant systems. I. Theory. IEEE Trans. on Aerospace and Electronic Systems, 1992, 28(4): 1056–1067.

[23] GAO P Y, LI K, SONG T X, et al. An accelerometers size effect self-calibration method for triaxis rotational inertial navigation system. IEEE Trans. on Industrial Electronics, 2017, 65(2): 1655–1664.

[24] ANDRADE-CETTO J, SANFELIU A. The effects of partial observability when building fully correlated maps. IEEE Trans. on Robotics, 2005, 21(4): 771–777.

[25] PERERA L D L, MELKUMYAN A, NETTLETON E. On the linear and nonlinear observability analysis of the SLAM problem. Proc. of the IEEE International Conference on Mechatronics, 2009: 1–6.

[26] KASSAS Z M. Analysis and synthesis of collaborative opportunistic navigation systems. Austin, U.S.A.: The University of Texas at Austin, 2014.

[27] KASSAS Z M, HUMPHREYS T E. Observability analysis of collaborative opportunistic navigation with pseudorange measurements. IEEE Trans. on Intelligent Transportation Systems, 2013, 15(1): 260–273.

[28] GUO Y F, THARMARASA R, KIRUBARAJAN T, et al. Passive coherent location with unknown transmitter states.

IEEE Trans. on Aerospace and Electronic Systems, 2017, 53(1): 148–168.
[29] BECKER K. Three-dimensional target motion analysis using angle and frequency measurements. IEEE Trans. on Aerospace and Electronic Systems, 2005, 41(1): 284–301.
[30] LI H W, WANG J. Particle filter for manoeuvring target tracking via passive radar measurements with glint noise. IET Radar, Sonar & Navigation, 2012, 6(3): 180–189.
[31] TOBIAS M, LANTERMAN A D. A probability hypothesis density-based multitarget tracker using multiple bistatic range and velocity measurements. Proc. of the 36th Southeastern Symposium on System Theory, 2004: 205–209.
[32] MOZYRSKA D, PAWLUSZEWICZ E, WYRWAS M. Local observability and controllability of nonlinear discrete-time fractional order systems based on their linearisation. International Journal of Systems Science, 2017, 48(4): 788–794.
[33] KASSAS Z, HUMPHREYS T. Observability analysis of opportunistic navigation with pseudorange measurements. Proc. of the AIAA Guidance, Navigation, and Control Conference, 2012: 1209–1220.
[34] HERMANN R, KRENER A. Nonlinear controllability and observability. IEEE Trans. on Automatic Control, 1977, 22(5): 728–740.
[35] KOTEICH M, MALOUM A, DUC G, et al. Local weak observability conditions of sensorless ac drives. Proc. of the 17th IEEE European Conference on Power Electronics and Applications, 2015: 1–10.
[36] ANGUELOVA M. Observability and identifiability of nonlinear systems with applications in biology. Goteborg, Sweden: Chalmers University of Technology and Goteborg University, 2007.
[37] CASTI J L. Recent developments and future perspectives in nonlinear system theory. Society for Industrial and Applied Mathematics Review, 1982, 24(3): 301–331.
[38] CHEN Z. Local observability and its application to multiple measurement estimation. IEEE Trans. on Industrial Electronics, 1991, 38(6): 491–496.
[39] RUGH W J. Linear system theory. 2nd ed. London: Prentice-Hall, 1996.
[40] HAM F M, BROWN R G. Observability, eigenvalues, and Kalman filtering. IEEE Trans. on Aerospace and Electronic Systems, 1983, 19(2): 269–273.
[41] KASSAS Z M, HUMPHREYS T E. Observability and estimability of collaborative opportunistic navigation with pseudorange measurements. Proc. of the Institute of Navigation GNSS Conference, 2012: 1–10.

Biographies

JING Tong was born in 1995. He received his B.S. degree in information countermeasure from Naval University of Engineering, Wuhan, China in 2017. He is currently pursuing his Ph.D. degree in communication and information system at Naval University of Engineering. His research interests are passive detection, passive coherent location, and signal processing.
E-mail: jingtong2018@yeah.net

TIAN Wei was born in 1984. He received his B.E. degree in communication engineering from Harbin Engineering University, China, in 2007, and Ph.D. degree in information and communication engineering from Tsinghua University, China, in 2014. He is now a postdoctor in the College of Electronic Engieering, Naval University of Engineering, China. His research interests include information fusion, radar signal processing and radar electronic warfare.
E-mail: tianwei09@tsinghua.org.cn

HUANG Gaoming was born in 1972. He received his B.S. and M.E. degrees in electronic warfare from Naval Electronic College of Engineering, China, in 1995 and 1998, respectively, and Ph.D. degree in signal processing from Southeast University, Nanjing, China, in 2006. He is currently the chief professor in Naval University of Engineering. His research interests are passive detection, intelligent signal processing, and electronic warfare system simulation.
E-mail: hgaom@163.com

PENG Huafu was born in 1987. He received his B.S. degree in electronic engineering and M.S. degree in information and communication engineering from Information Engineering University, Zhengzhou, China, in 2008 and 2013, respectively. He is currently pursuing his Ph.D. degree in mechanical engineering at Naval University of Engineering. His research interests are information fusion and communication signal processing.
E-mail: huaf_peng@163.com